

Contents lists available at ScienceDirect

Polymer

journal homepage: http://www.elsevier.com/locate/polymer





Shape memory Poly(lactic acid) binary blends with unusual fluorescence

Shuai Zhang ^a, Tuan Liu ^{a,**}, Baoming Zhao ^a, Christina Verdi ^{a,b}, Wangcheng Liu ^a, Cheng Hao ^a, Jinwen Zhang ^{a,*}

- a School of Mechanical and Materials Engineering, Composite Materials and Engineering Center, Washington State University, Pullman, WA, 99164, USA
- ^b College of Natural Resources, North Carolina State University, Raleigh, NC, 27607, USA

ARTICLE INFO

Keywords:
Catalyst free
Poly(lactic acid)
Clusterization-triggered emission
Shape memory
Toughening
Vitrimer

ABSTRACT

A multifunctional PLA blend with shape memory, fluorescence and improved toughness is prepared via reactive compounding of a multifunctional prepolymer (GSE) with PLA in the absence of an external catalyst. GSE is synthesized by glycerol-mediated bulk polymerization of succinic anhydride and ethylene glycol diglycidyl ether, and its self-crosslinking reaction taking place during compounding introduces an elastomeric polymer dispersed in the PLA matrix. The transesterification at the interface compatibilizes the PLA blend resulting in significantly improved toughness. Moreover, the resulting PLA blend exhibits strong fluorescence, and the fluorescence intensity of the PLA blend with 40% GSE is stronger than that of neat crosslinked GSE. The PLA blend also exhibits an excellent shape memory property, explained by the improved toughness for larger deformation and the crosslinked GSE-rich phase for the storage of internal stress induced by deformation. This work introduces a new preparation method for a smart PLA material with improved toughness, strong fluorescence, and shape memory by simple melt compounding of PLA and a multifunctional modifier (GSE).

1. Introduction

PLA is a renewable thermoplastic that has found many applications such as packaging, textile, 3D printing, biomedical devices, etc., yet it only accounts for a small fraction of the polymer materials market that is dominated by petroleum-based thermoplastics. This is because PLA is limited by its relatively high cost in addition to its brittleness and low heat resistance. Developing smart PLA materials may apply PLA for higher value products and increase its market share. In the past decades, smart polymers with multifunctional properties, such as shape memory and fluorescence, have received extensive attention and demonstrated applications in the areas of medical devices, smart textile, biosensor, etc.

Shape memory polymers (SMPs) are a class of smart materials which recover from a deformed (temporary) shape to original (permanent) shape upon external stimulation. The thermally responsive SMPs are the most studied ones. Conventional thermally responsive SMPs possess chemically or physically crosslinked network structures composed of stiff and soft segments [1]. Many linear thermoplastic polymers do not have this characteristic and hence are not SMPs. In recent years, many shape memory PLA materials have been prepared via reactive compounding of PLA with a flexible component to establish reactive

compatibilization at interface. For example, Tsujimoto et al. reported a shape memory PLA material by crosslinking of epoxidized soybean oil in PLA matrix in presence of a benzylsulfonium-based cationic catalyst [2]. In another example, Chen et al. prepared a shape memory PLA by blending PLA and natural rubber (NR) presence of a peroxide that induced the crosslinking of NR and reaction of NR and PLA at interface [3]. In both cases, the brittle PLA was toughened by an in situ crosslinked elastomer to afford large deformation and good shape recovery of the resulting materials. The authors also pointed out that a strong interfacial compatibilization between the crosslinked rubber phase and PLA phase was crucial to obtain good mechanical properties. Reactive compatibilization usually relies on catalysts for activating and promoting the chemical reaction between polymer matrix and modifier [3–5]. Those catalysts are tertiary amines, metal salts and peroxides which may bring toxicity to the polymer blends. Therefore, it is desirable to prepare shape memory PLA by catalyst-free reactive compounding.

On the other hand, fluorescent organic compounds have received extensive investigations due to their sensitive responses to temperature, metal ions and pH value. Conventional light emitting organic compounds are used in solution rather than in solid, because the fluorescence is quenched in solid state. Light emitting organic compounds

E-mail addresses: tuan.liu@wsu.edu (T. Liu), jwzhang@wsu.edu (J. Zhang).

^{*} Corresponding author.

^{**} Corresponding author.

which follows aggregation induced emission (AIE) mechanism can be used in solid state and has been used as additive in polymer materials for detecting the corrosion of a metal substrate and monitoring the swelling process of a hydrogel [6-8]. In these works, the AIE compounds are conjugated small molecules and used as additive rather than major component in polymer materials. This may be because the organic compounds with such rigid structure may suffer from serious steric hindrance for polymerization. In the recent decade, a class of polymer with intrinsic fluorescence named non-traditional fluorescence compounds (NTFCs) have been discovered [9]. NTFCs usually possess highly branched structure with no conjugated structural unit. Hyperbranched poly (amidoamine) [10,11], polysiloxanes [12,13], poly (phosphate) [14], polyether [15], and polyester [16,17] are some examples of NTFCs which emit fluorescence via clusterization-triggered emission (CTE) mechanism. These NTFCs usually possess high molecular weight and reactive functional groups, making them readily used as major component in polymer materials. Conventional thermoplastics (e.g., poly (ethylene oxide) (PEO) and PLA) show negligible or no fluorescence. We assume that introducing NTFCs to thermoplastics would provide fluorescence property to the resulting materials.

In this work, a PLA-based shape memory and fluorescent material was prepared via a facile and green approach. First, glycerol, succinic anhydride (SA) and ethylene glycol diglycidyl ether (EGDE) were reacted to give a prepolymer named "GSE" (Scheme 1) which was subsequently compounded with PLA to yield a PLA blend with fluorescence and shape-memory properties. Both self-crosslinking of GSE and transesterification between GSE and PLA took place during compounding without a catalyst. The resulting blend exhibited good compatibility and retained good melt processability. In addition, the inclusion of a soft crosslinked GSE phase in PLA matrix not only improved the toughness of PLA, but also provided shape memory property to the PLA/GSE blends. More interestingly, PLA/GSE blends emitted blue fluorescence via the CTE mechanism.

2. Experimental section

2.1. Material

PLA 3052D (NatureWorks), glycerol (TCI, 99%), ethylene glycol diglycidyl ether (EGDE, epoxy value = 0.76 mol 100 g $^{-1}$, TCI), succinic

anhydride (SA, ACROS, 99%), chloroform-d (CDCl $_3$, Aldrich, 99.8%), dimethyl sulfoxide-d (DMSO- d_6 , Aldrich, 99.9%), silicon dioxide (Aldrich, 5–15 nm), and all solvents (GR grade) were used without further purification.

2.2. Synthesis of GSE

Glycerol (35 g), SA (38 g), and EGDE (100 g) were added into a 500 mL round bottom flask and reacted under magnetic stirring at 130 $^{\circ}$ C for 1 h and 150 $^{\circ}$ C for 40 min. The molar ratio of glycerol monomer, SA monomer, and epoxy group of EGDE was fixed at 0.5:0.5:1.

2.3. Preparation of PLA/GSE blends

- 1) Melt compounding: PLA pellets were dried in a vacuum oven at 80 °C for 12 h. The dried pellets were loaded into a micro twin-screw extruder (Haake Minilab) at 185 °C. When the pellets were totally melted, GSE was added and then compounded with PLA at 185 °C for 10 min with a screw speed of 100 rpm. Table 1 shows the formulations of PLA/GSE blends containing 0, 10, 20, 30 and 40wt% of GSE, respectively.
- 2) Injection molding: The samples for tensile and DMA tests were prepared using a mini injection molding machine (Haake minijet II). The cylinder and the mold were preheated to 190 $^{\circ}$ C and 40 $^{\circ}$ C, respectively. The samples from melt compounding were loaded into the cylinder and melted at 190 $^{\circ}$ C for 180 s. The melted samples were injected into the mold. The injection pressure was 600 bar, and the injection time was 15 s. The post pressure was 150 bar, and the holding time was 20 s.
- 3) Film preparation: Film samples were prepared using a hot press (Carver, 3693-230). The samples (\sim 2 g) from melt compounding were loaded into a Teflon mold with a dimension of 16 cm \times 8 cm \times 0.25 mm (Fig. S1) and placed in the hot press. The samples were pressed at 190 °C for 5 min.

2.4. Characterizations

The molecular weight of GSE was measured using a gel permeation chromatography (GPC, Viscotek) system equipped with a GPCmax $^{\text{TM}}$ Pump/Autosampler/Degasser Module and a TDA 305 multi-detector. A

Scheme 1. Synthesis route of GSE using glycerol, succinic acid (SA) and ethylene glycol diglycidyl ether (EGDE) as reactants. The mass ratio of glycerol, SA, and EGDE is 35/38/100 which is equivalent to a molar ratio of –OH, anhydride and epoxy group of 1.5/0.5/1. The digital photo shows GSE is transparent and colorless.

Table 1 Formulations of PLA/GSE blends and their thermal properties.

Sample	GSE content	Gel content	DSC (°C) ^a		DMA (°C) ^b		TGA (°C)
	(wt%)	(%)	^a T _g ,	^b Tg,	cTg,	$^dT_{\mathrm{g},}$	$^eT_{ m d5}$
			GSE	PLA	GSE	PLA	
PLA	0	NA	NA	56.2	-	63.2	315
PLA/	10	4.4 \pm	-26.2	53.6	-19.4	59.8	319
GSE-		0.5					
10							
PLA/	20	12.4 \pm	-26.2	52.8	-19.4	58.6	315
GSE-		0.6					
20							
PLA/	30	22.5 \pm	-26.4	52.6	-19.7	58.3	304
GSE-		0.8					
30							
PLA/	40	31.9	-26.0	52.2	-19.8	58.0	303
GSE-		± 1.6					
40							

 $^{^{\}rm a}~T_{\rm g,~GSE}$ and $T_{\rm g,~PLA}$ values are the $T_{\rm g}$ of the crosslinked GSE-rich phase and the PLA-rich phase in PLA/GSE blends measured by DSC;

HPLC grade tetrahydrofuran (THF) was used as eluent with a flow rate of $1.0~\rm mL~min^{-1}$. Fourier transform infrared (FTIR) spectra were collected using a NICOLET iS50 FTIR spectrometer. The sample was scanned from 400 to 4000 cm⁻¹ for 64 times with a resolution of 4.0 cm⁻¹. Nuclear magnetic resonance (NMR) spectra were recorded on a Varian 400-NMR spectrometer (400 MHz). CDCl₃ or DMSO- d_6 was used as the deuterated solvent. Chlorobenzene (20 mg) was added into 1 mL CDCl₃ as an internal standard.

The curing behavior of GSE was monitored using a Discovery HR-2 rheometer (TA Instruments) equipped with a pair of 25 mm parallel plates. The sample was scanned at 150 °C with a constant frequency of 10 rad s $^{-1}$ and a constant strain of 0.5%. The changes of storage modulus ($G^{\prime\prime}$), loss modulus ($G^{\prime\prime}$), and complex viscosity of the PLA/GSE blends with temperature were recorded. In the temperature sweep measurements, samples were heated from 100 to 200 °C at a heating rate of 3 °C min $^{-1}$ with a constant frequency of 10 rad s $^{-1}$ and a constant strain of 0.5%. In the frequency sweep measurements, samples were scanned from 0.1 to 500 rad s $^{-1}$ at 190 °C with a constant strain of 0.5%. For all rheological tests, the gap was 1000 μm .

The T_g and curing behavior were monitored using a differential scanning calorimeter (DSC1, Mettler-Toledo). The sample (~5 mg) was sealed in an aluminum crucible and scanned from -50 to $280~^{\circ}\text{C}$ at a heating rate of 5 °C min⁻¹ under nitrogen atmosphere. Thermal stability was measured using a thermo-gravimetric analyzer (TGA/DSC1, Mettler-Toledo). The sample (\sim 10 mg) was scanned from 50 to 800 $^{\circ}$ C at a heating rate of 10 °C min⁻¹ under nitrogen atmosphere. Dynamic mechanical properties were tested using a dynamic mechanical analyzer (Q800 DMA, TA Instrument) in single cantilever mode. The specimen with a dimension of $\sim\!35$ mm \times 10 mm \times 1 mm was scanned from -50to 150 °C at a heating rate of 3 °C min⁻¹. The oscillation amplitude was 15 μm, and the frequency was 1 Hz. Tensile property was tested based on ASTM D638 using type V dog bone samples. The test was carried out on a universal test machine (Instron 4466) equipped with a 10 KN electronic load cell. The crosshead speed was 1 mm min⁻¹. The strain was monitored by clamping a 1.0-inch extensometer (MTS 634.12E-24) on the test sample. For each formulation, at least five specimens were tested.

Luminescence experiments were carried out using a Cary Eclipse Fluorescence Spectrophotometer (Agilent Technologies). Samples were prepared to be rectangular films with a dimension of 1 cm \times 1 cm \times 0.25 mm. The fluorescence spectra were scanned from 380 to 700 nm at an excitation wavelength of 365 nm. The slit width was set as $E_{\rm x}=10$, $E_{\rm m}=10$. UV–Vis absorption spectra of GSE and the crosslinked GSE with

a thickness of 0.25 mm were measured using a PerkinElmer spectrometer (Lambda 25). The samples were scanned from 200 to 600 nm.

The gel content of PLA/GSE blends was measured via the solvent extraction method according to ASTM D2765-16. Samples were dried in a vacuum oven at 80 °C for 24 h to remove the volatiles. In a 250 mL round bottom flask equipped with a Soxhlet extractor, the dried sample ($\sim 0.300 \pm 0.020$ g, W_1) was extracted by 100 mL of xylene for 12 h. After extraction, the swollen sample was dried in a vacuum oven at 100 °C until a constant weight (W_2) was obtained. At least three repeats were performed for each formulation. The gel content was calculated according to the following equation,

$$Gel\ content\ (\%) = \frac{W_2}{W_1} \times 100\% \tag{1}$$

3. Results and discussion

3.1. Synthesis of GSE

Glycerol was introduced to the SA/EGDE reaction system (Scheme 1) to afford a catalyst-free preparation of GSE. It is understood that hydroxyl groups present in the reaction system play a critical role in the curing of epoxy with anhydride in absence of an external catalyst, and polyhydric compounds can serve as internally catalytic species [18,19]. In a recent study, our group utilized glycerol as a co-monomer to prepare a catalyst-free epoxy vitrimer [20]. It was noted that the high polarity glycerol was immiscible with the SA/EGDE mixture at room temperature, but the mixture turned to a clear and transparent glycerol-SA-EGDE (G-S-E) solution at 130 °C (Fig. S2). Fig. S3 shows the DSC heating curve of a well-mixed G-S-E solution. A broad exothermic peak attributed to the curing reaction appeared at 100-250 °C. In the second heating curve, the T_g of the cured GSE appeared at ~ -5 °C (Fig. S4). The low T_g was due to the flexible structures of the building blocks. To acquire a moderate reaction rate, polymerization was performed at 150 °C. Fig. 1a shows the change of complex viscosity (η^*) during the polymerization at 150 °C. The viscosity of the G-S-E solution started to increase dramatically at ~40 min due to the increase of molecular weight as demonstrated from the GPC curves (Fig. 1b). The gel point is the time when storage modulus (G') and loss modulus (G'') intersect. The reaction mixture started to turn to gel at ~47 min (Fig. 1a). Therefore, the reaction time of synthesis of GSE was set at 40 min to achieve a decent molecular weight and also avoid gel formation. GSE obtained was a colorless and viscous liquid with a viscosity of $\sim\!288$ Pa s at 25 $^{\circ}\text{C}$. Fig. 1c and Fig. S5 show the ¹H NMR spectra of GSE and the reactants. Both the peak for SA at 2.88 ppm and the peaks for glycerol at 3.4 ppm and 3.25 ppm disappeared after polymerization. A new peak at 12.2 ppm corresponding to carboxylic acid (-COOH) groups appeared. The peaks at 2.7 and 3.1 ppm corresponding to epoxy groups decreased for ~70%. Epoxy value and acid value of GSE were found to be 0.109 mol/100 g and 0.120 mol/100 g via titration, respectively.

3.2. Compounding of PLA/GSE and rheological properties of the resulting blands

Fig. S6 shows the torque value versus time during compounding of neat PLA and PLA/GSE-30 (i.e., GSE is 30 wt% on the basis of total mass) in a torque rheometer, respectively. Data was collected at 185 °C. After PLA was melted (at \sim 2 min), the torque value of the PLA melt largely remained constant, indicating it is thermally stable at the temperature and time frame. In contrast, the torque value of PLA/GSE-30 melt started to increase at \sim 5 min of mixing, which was due to the crosslinking of GSE (Fig. S7) and the likely reaction of GSE and PLA at the interface as well [21]. Fig. S8 shows the change of gel content of PLA/GSE-30 with compounding time. The gel content changed from 15.7% at 5 min of compounding to \sim 22.5% at 10 min, and further increase in compounding time did not result in obvious increase in gel content.

 $^{^{\}rm b}$ $T_{\rm g,~GSE}$ and $T_{\rm g,~PLA}$ are obtained from the peak temperatures of tan δ curves; $^{\rm c}$ $T_{\rm d5}$ is the temperature at 5% weight loss obtained from the TGA heating curve.

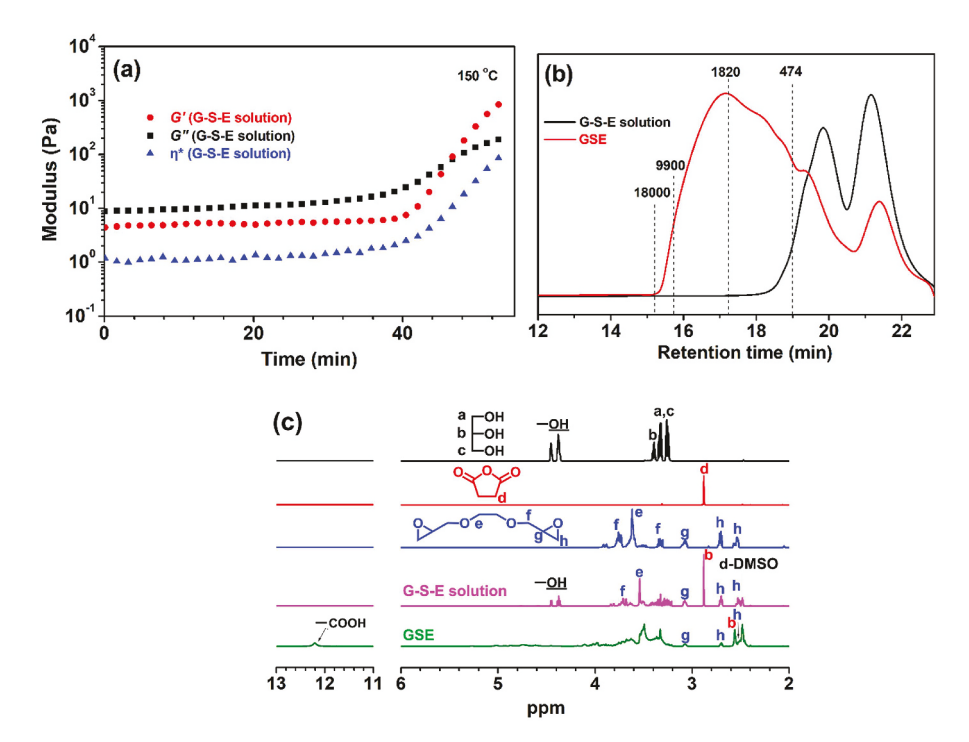


Fig. 1. (a) Changes of G', G'', and η^* of the glycerol-SA-EGDE ("G-S-E") solution with reaction time at 150 °C; (b) GPC curves of G-S-E solution and GSE. The dash line indicates the molecular weight (M_p) of standard polystyrenes. Compared with that of G-S-E solution, the major peak of GSE shifted to lower retention time indicating the increase of molecular weight; (c) ¹H NMR spectra of glycerol, SA, EGDE, G-S-E solution, and GSE.

Considering the efficiency and potential thermal degradation at high temperature, all the PLA/GSE blends for the rest of experiments were prepared with 10 min of compounding. Fig. S9 shows the gel contents of the PLA blends with different GSE contents. The gel content increased almost linearly with the increase in GSE loading. The insoluble gel of

PLA/GSE-30 obtained from the extraction experiment was collected and hydrolyzed in 0.1 N hydrochloric acid. Fig. S10 shows the comparison of ¹H NMR spectra of GSE, PLA and the hydrolyzed gel. The result indicates the gel phase of the blend was mostly composed of the crosslinked GSE. However, the signals at 1.58 and 5.15 ppm attributed to PLA were also

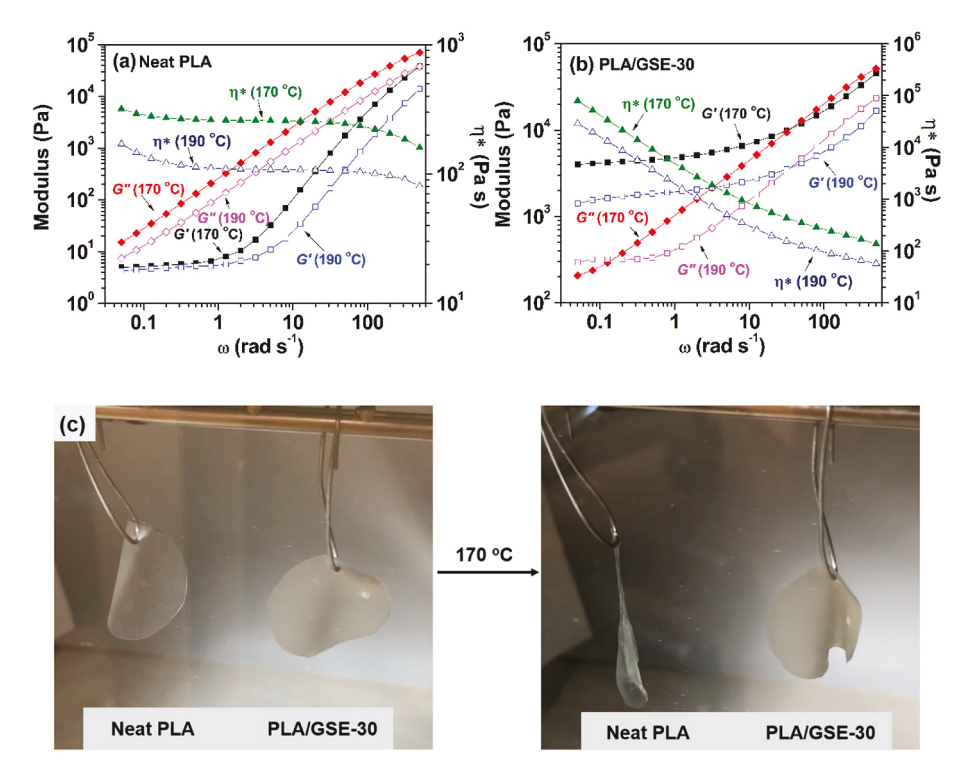


Fig. 2. Changes of storage modulus (G''), loss modulus (G'') and complex viscosity (η^*) of the prepared (a) neat PLA and (b) PLA/GSE-30 with frequency ranging from 0.05 to 500 rad s⁻¹ at 170 °C and 190 °C, respectively; (c) digital photos of PLA and PLA/GSE-30 in a convection oven at 170 °C. After 30 s, the PLA/GSE-30 film (right) still hanged on the shelf; while the neat PLA film (left) melted down.

noted in the ¹H NMR spectrum of the hydrolyzed gel. This result indicates that crosslinked GSE constituted the dispersed phase in the blend, and the reaction between GSE and PLA also occurred via transesterification at the interface during compounding. Fig. S11 shows the GPC curves of PLA and PLA/GSE blends. The gel was filtered before test. It is noted that the molecular weight of PLA phase in PLA/GSE blends almost remained unchanged (Table S1) indicating that the hydroxy-rich GSE did not cause hydrolysis of PLA during compounding.

Fig. 2a and b shows the changes of rheological properties of neat PLA and PLA/GSE blends with frequency ranging from 0.05 to 500 rad s^{-1} . Data was collected from 170 to 190 $^{\circ}\text{C},$ respectively. The η^{*} of neat PLA melt (Fig. 2a) did not change obviously at frequency below 10 rad s^{-1} . As frequency increased further, η^* started to decrease, and the melt displayed shear thinning due to the disentanglement of polymer chains. This is a typical rheological behavior for most pure polymers. With the addition of GSE, the melt of the PLA/GSE blend exhibited shear thinning in the whole frequency range of test. In addition to establishing reactive interfacial compatibilization with PLA by covalent bonds, the hydroxyrich GSE can also form H-bonding with PLA which is sensitive to shear stress. Therefore, all PLA/GSE blends exhibited shear thinning at even low frequency due to the disturbing of H-bonding and the terminal phenomenon increasingly departed from the Newtonian fluid behavior with GSE loading (Fig. S12). It is interesting to note that at low GSE loading the melt of PLA/GSE-10 exhibited a slightly lower η^* with respect to that of neat PLA. This was because the plasticizing effect of the uncrosslinked GSE in PLA/GSE-10 outweighed the effect of the crosslinked GSE. At higher GSE loading, however, the PLA/GSE blends displayed increasingly higher η^* than the neat PLA, which is due to the increased gel fraction in PLA/GSE blends.

In addition, at low frequency (0.1 rad s⁻¹) neat PLA melt exhibited a

fluid-like behavior, i.e., G'' > G', and the melt of PLA/GSE-10 blend showed a similar behavior though G' was slightly higher than that of neat PLA. G' is a measure of the elasticity and strength of polymer material melt, while G'' is related to the energy dissipation owing to molecular mobility in melt. It is noted that G' of the blend increased steadily with the GSE content. When GSE loading increased to above 20%, the PLA/GSE blends exhibited a solid-like behavior as G' were higher than G''. These results indicated the formation of crosslinked network in the blend [22]. Video S1 and Fig. 2c show the PLA and PLA/GSE-30 films in a convection oven. After heating at 170 °C for 30 s, the neat PLA film melted down, while the PLA/GSE-30 film retained its original shape due to its solid-like behavior at 170 °C. However, the PLA/GSE-30 film melted down after heating for 1 min.

Supplementary data related to this article can be found at https://doi.org/10.1016/j.polymer.2020.122980.

3.3. Thermal and mechanical properties of PLA/GSE blends

Results from both DMA (Fig. 3a and b) and DSC (Fig. S13) experiments demonstrate the existences of two glass transitions for all the PLA/GSE blends, suggesting the phase-separated structure of the blends. The transition at the lower temperature is associated with the cross-linked GSE-rich phase, while the one at the higher temperature is attributed to the PLA-rich phase. Table 1 lists the measured glass transition temperatures ($T_{\rm g}$'s) associated with individual phases. DMA test generally yields higher $T_{\rm g}$ values than DSC test, which is a methodological phenomenon. It is noted that the $T_{\rm g}$ associated with the GSE-rich phase showed little change with blend composition, suggesting that this phase was basically composed of crosslinked GSE. Neat PLA displayed a $T_{\rm g}$ of ~56 °C (DSC), in contrast, the $T_{\rm g}$ associated with the PLA-rich

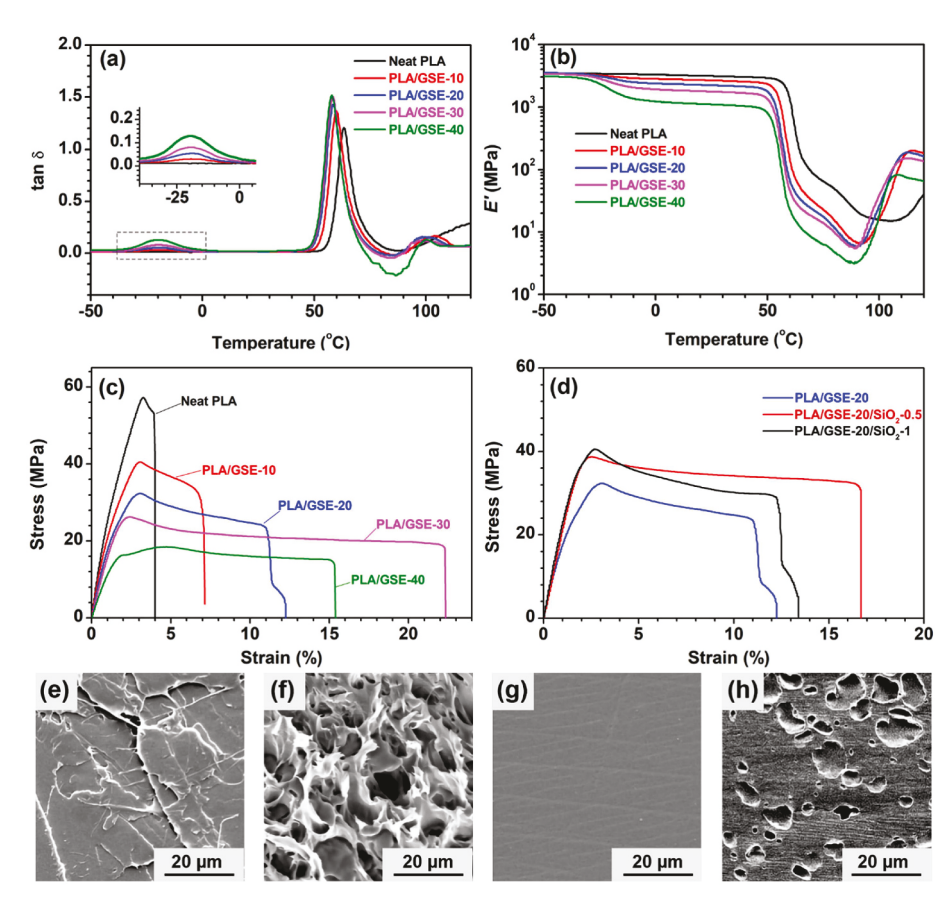


Fig. 3. (a) tan δ curves and (b) storage modulus curves of PLA and PLA/GSE blends vs. temperature; (c) stress-strain curves of PLA and PLA/GSE blends; and (d) stress-strain curves of PLA/GSE-20 blends containing different amounts of nano silica; (e) & (f) SEM images of tensile-fractured surfaces of neat PLA and PLA/GSE-30; (g) & (h) SEM images of cryo-fractured surfaces of neat PLA and PLA/GSE-30.

phase in PLA/GSE blends displayed a decreasing trend with increase in GSE loading (Table 1). Because the molecular weight of the PLA-rich phase remained almost unchanged (Fig. S11), the decrease in $T_{\rm g}$ was probably due to the flexibilizing effect of GSE that was dissolved in the PLA phase.

PLA/GSE blends demonstrated very similar dynamic mechanical properties like many other PLA blends with flexible polymers or rubbers [23]. In the glass transition region of the GSE phase, the PLA/GSE blend displayed obvious reduction in storage modulus (E') that was kind of proportional to the GSE content in the blend (Fig. 3b), which can be explained by the presence of flexible GSE in the blend. In the glass transition region of PLA, the blend experienced a drastic drop in E', which was mainly attributed to the amorphous nature of the continuous PLA phase in the blend. Because of its slow crystallization rate, the semi-crystalline PLA often presents in amorphous form. DSC results (Fig. S13 and Table S2) revealed the approximate equality of enthalpy of fusion to that of cold crystallization, suggesting that the PLA in the blends was basically amorphous. The cold crystallization during testing was also reflected in the recovery of E' for neat PLA and its blends as the temperature increased further after PLA was in its rubbery state (Fig. 3b). The crosslinked GSE promoted the cold crystallization of PLA as reflected in the lower cold crystallization temperatures seen in both the DSC thermograms and the change of E' with temperature in the DMA

Neat PLA exhibited a brittle failure with an elongation at break of ~3.7%, while PLA/GSE blends exhibited a ductile behavior showing a continuous increase of elongation at break with GSE content (Fig. 3c). Accordingly, the tensile-fractured surface of PLA (Fig. 3e) was relatively smooth suggesting brittle failure, while the fractured surface of PLA/ GSE-30 (Fig. 3f) was much rougher suggesting extensive plastic deformation involved in the fracture process. Nonetheless, the improvement in ductility of PLA by GSE was moderate in comparison with the properties of many other polymer modifier toughened PLA blend systems. Fig. S14 shows that all the tested samples displayed tensile whitening across the gauge length without a clear necking, suggesting the improved ductility was mainly from the extensive crazing during tensile test [24-26], which was also consistent with the appearance of plastic deformation shown in Fig. 3f. Fig. 3h shows a clear phase-separated morphology for PLA/GSE-30. The dispersed domain size ranged from 5 to $25 \mu m$. The lower ductility in this study was probably related to the particular phase structure and relatively large domain sizes of the dispersed phase in PLA. The size and the dispersity of GSE in PLA is determined by many factors such as compatibility between GSE and PLA, GSE loading, and compounding conditions (i.e., temperature, time, and screw speed). To achieve monodispersed particles and a better mechanical performance of the polymer blends, these factors should be considered and investigated in the future study.

On the other hand, both tensile strength and modulus of PLA/GSE blends decreased with increase in GSE content (Table 2), which was similar to the behaviors of many other reactive compatibilized PLA blends with flexible/soft polymers [27–29]. To offset the reductions of tensile strength and modulus associated with addition of GSE, nano silica (SiO $_2$, 5–15 nm) was incorporated during the synthesis of GSE, and

Table 2Tensile properties of PLA and PLA/GSE blends.

Sample	Strength (MPa)	Modulus (GPa)	Elongation at break (%)
PLA	57.9 ± 0.6	3.5 ± 0.1	3.7 ± 0.2
PLA/GSE-10	40.0 ± 0.5	3.1 ± 0.1	7.5 ± 0.8
PLA/GSE-20	32.4 ± 0.1	2.5 ± 0.1	11.1 ± 1.1
PLA/GSE-30	26.0 ± 0.5	2.2 ± 0.2	23.5 ± 1.9
PLA/GSE-40	19.0 ± 0.5	1.6 ± 0.1	13.9 ± 1.3
PLA/GSE-20/SiO2-	37.7 ± 0.6	3.2 ± 0.2	15.9 ± 0.8
0.5			
$PLA/GSE\text{-}20/SiO_2\text{-}1$	38.7 ± 1.6	2.5 ± 0.1	13.3 ± 1.0

the resulting nano silica containing GSE was blended with PLA to receive reinforced blends. Compared with PLA/GSE-20, the blend PLA/G-SE-20/SiO₂-0.5 (containing 0.5 wt% of nano silica based on the total weight of polymer blend) exhibited increases of 16.4, 28.0, and 43.2% for strength, modulus, and elongation at break, respectively (Fig. 3d, Table 2). These results indicate that nano silica at a low loading level is fairly effective to improve the overall mechanical performance. Nano silica alone has been well demonstrated as an effective modifier for the improvements of the mechanical properties of PLA and its polymer blends [30,31]. Nano silica possesses larger surface area and excellent compatibility with polymers. At low loading levels, the strong interaction between nano silica and polymer matrix could prevent the growth of the crack, which leads to the increase of energy absorption during the mechanical tests and results in the improvements of the mechanical properties of the polymer blend. In addition, the rigid structure of nano silica could also contribute to the improvements of strength and modulus. During the preparation of nano silica containing blends, nano silica was introduced in the synthesis of GSE, meaning that GSE was prepared in presence of nano silica. Because the hydroxyl groups on the surface of nano silica might participate in the reaction [32], the dispersion of nano silica in the blend system may be a complicated situation. Nano silica and GSE may both present as individual dispersed phases in PLA and/or exist in a nano silica core-GSE shell structure dispersed in the PLA phase. Therefore, PLA toughening is achievable in either case, and a balanced performance can be achieved as seen in many reports. It should be mentioned that the mechanical properties did not increase further with increase of nano silica loading up to 1 wt%. This was probably because at high loading levels, aggregation of nano silica particles and the decrease of polymerization rate of GSE compromises the reinforcing and toughing effects (Fig. S15 and S16), leading to the decrease of the mechanical properties of the polymer blend.

3.4. Shape memory of PLA/GSE blends

Prior to testing the shape memory property, the rectangular film sample with a dimension of \sim 80 mm \times 5 mm \times 0.25 mm was deformed to "U" shape at 80 °C in a convection oven. Subsequently, the "U" shaped film was wrapped with an aluminum foil to fix the shape. The sample was then put in a convection oven at 150 °C for 1 h. The aluminum foil was removed from the sample, and the permanent shape of the film sample turned to "U" shape due to the plasticity provided by PLA. To investigate the shape memory property, the film with "U" permanent shape was flattened at 80 °C and quickly cooled down to room temperature to fix the temporary "-" shape. The shape fixity (Rf) was calculated following Eq. (2), where θ_i represents the angle of the film after shape fixing (Fig. 4a). The $R_{\rm f}$ values of all the samples were above 97.8% (Table S3) and comparable to that of other PLA based shapememory materials [33,34]. This result indicates the shapes of all samples were successfully fixed. The temporary "-" shape was then recovered to the "U" shape at 80 °C in a convection oven. The recovered angle (θ_r) was recorded by a camera (Fig. 4a). The shape recovery ratio $(R_{\rm r})$ was calculated according to Eq. (3).

$$Rf = \frac{\theta_i}{180^\circ} \times 100\% \tag{2}$$

$$R_r = \frac{\theta_i - \theta_r}{\theta_i} \times 100\% \tag{3}$$

Fig. 4b shows the $R_{\rm r}$ vs. time for PLA and the PLA/GSE blends. Neat PLA exhibited a certain shape memory property, and the maximum $R_{\rm r}$ value was only ~78%. The shape memory of neat PLA is because (1) the physical entanglements of long PLA chains for the storage of internal stress, and (2) the polymer chains between the entanglements can be stretched to afford deformation [35,36]. Most reported SMPs possess a $R_{\rm r}$ value above 90%, therefore the shape memory property of PLA is poor. As the increase in GSE content, both the maximum $R_{\rm r}$ value and

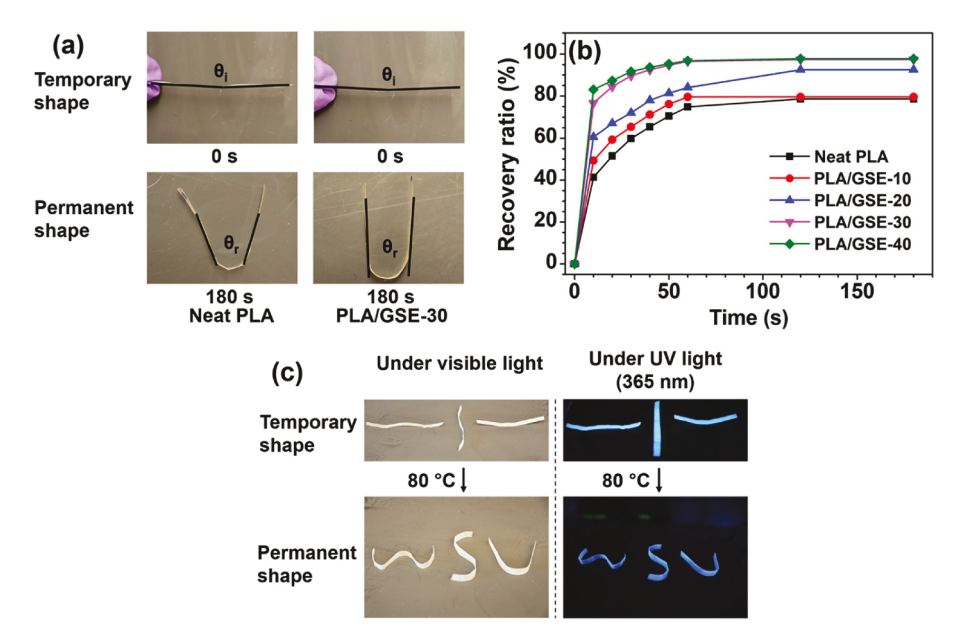


Fig. 4. (a) Shape recovery of neat PLA and PLA/GSE-30 for the testing of recovery ratio; (b) Shape recovery ratio of PLA/GSEs as a function of time at 80 °C; (c) Shape memory images of PLA/GSE-30 under visible light (left) and UV light (right, 365 nm).

the shape recovery rate increased. PLA/GSEs -30 and -40 exhibited a maximum $R_{\rm r}$ of \sim 97%, and their shape was recovered for \sim 80% in just 10 s, indicating their satisfactory shape memory property. The $R_{\rm f}$ values of PLA/GSEs -30 and -40 are also comparable to that of other reported PLA based shape memory materials [2,37]. Fig. 4c and Video S2 provide a visualized version for the shape memory behavior. At the beginning, PLA/GSE-30 films with permanent shape of "W–S–U" were flattened at above $T_{\rm g}$. Upon cooling below $T_{\rm g}$, the temporary shape of the films was fixed. Subsequently, the PLA/GSE-30 films were moved to a heating plate with a temperature of 80 °C (above $T_{\rm g}$) to allow the quick recovery of the shape to "W–S–U". The satisfactory shape memory property of PLA/GSE blends could be related to the following reasons: (1) the crosslinked GSE temporally stored the internal stress induced by deformation; (2) the reactive compatibilization at interface facilitied the efficient transfer of the stress between the two phases during the shape

deformation and recovery; (3) the PLA/GSE blends possessed a lower rubbery modulus (Fig. 3b) than neat PLA, so less stress was needed during the shape recovery. Fig. 4c shows the shape memory of PLA/GSE-30 under UV lamp (365 nm), and strong blue fluorescence was emitted from the PLA/GSE-30 film, which will be further discussed in the next section.

Supplementary data related to this article can be found at https://doi.org/10.1016/j.polymer.2020.122980.

3.5. Light emission of PLA/GSE blends

Neat PLA only emits negligible fluorescence (Fig. 5a). After compounded with GSE, the resulting PLA/GSE blends displayed a stronger fluorescence intensity which increased with GSE concentration (Fig. 5b). This result indicated that the fluorescence behavior was

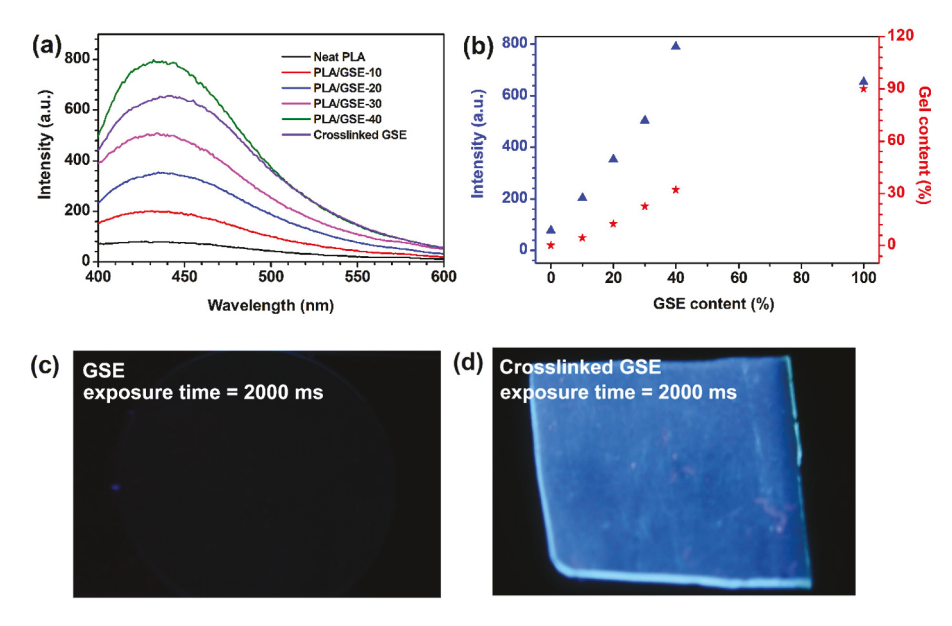


Fig. 5. (a) Fluorescence spectra of PLA blends and crosslinked GSE (0.25 mm films); (b) The changes of fluorescence intensity and gel content with GSE content; digital photos of (c) GSE and (d) crosslinked GSE film under UV lamp (365 nm). The images were taken from Nikon D3200 camera with the exposure time of 2000 ms, the aperture of f/4.0, and the ISO of 100.

largely related to the crosslinked GSE phase. To better understand the fluorescence behavior, the change of fluorescence intensity of GSE before/after self-crosslinking were investigated. First, none of the starting monomers for GSE preparation (glycerol, EGDE and SA) exhibits any fluorescence (Fig. S17). The GSE before crosslinking exhibited a weak light absorption in the range of 300–400 nm (Fig. S18) and emitted no fluorescence under UV light (365 nm) (Fig. 5c and S19). After self-crosslinking, the resulting GSE film (~0.25 mm in thickness) showed greatly enhanced light absorption (Fig. S18) and strong fluorescence emission (Fig. 5d). These results indicate that the strong fluorescence from PLA/GSE blends is derived from crosslinked GSE phase. Similar polymerization or crosslinking triggered fluorescence was also reported by Zhu et al. and Liu et al. [38,39]. The crosslinking reaction bonded the GSE molecules together as a whole to yield a significantly enhanced CTE phenomenon (Fig. S20).

It is worth noting that PLA/GSE-40 emitted even stronger fluorescence than the neat crosslinked GSE (Fig. 5a and b), indicating that the polyester structure of PLA is capable of enhancing the CTE effect. This phenomenon is further proved by the changes of fluorescent intensity and gel content with GSE loading from Fig. 5b. It is noted that the gel content, ascribed to the crosslinked GSE-rich phase, has a linear correlation with GSE loading. If the fluorescence intensity was simply the sum of the one part from the GSE-rich phase and the other part from PLA-rich phase, the fluorescence intensity changed with GSE loading would be linear. However, the results showed the fluorescence intensity of all the PLA/GSE blends were higher than the linearly predicted values, indicating that the compatibilized interphase between the PLA and GSE phase promotes the clusterization phenomenon which enhances the fluorescence intensity (Fig. 6). Therefore, reactive compounding is believed to be a facile strategy to convert PLA to fluorescent polymer by taking advantage of the enhanced CTE effect.

4. Conclusions

A multifunctional prepolymer (GSE) was prepared by bulk

polymerization of glycerol, succinic anhydride and ethylene glycol diglycidyl ether in a catalyst-free and solvent-free process. The prepared GSE was then compounded with PLA. Because GSE contained epoxy groups, carboxyl groups and hydroxyl groups, it could undergo selfcatalyzed crosslinking during compounding with PLA and enable reactive compatibilization at interface between GSE and PLA. The crosslinked GSE was elastomeric and dispersed in PLA. The PLA/GSE blends exhibited notable improvement in ductility but reductions in strength and modulus. To offset the reductions of strength and modulus, nanosilica was added during the compounding process. With addition of 0.5 wt% nano silica to the PLA/GSE-20 blend, and strength, young modulus, and elongation were respectively improved by 16.4, 28.0 and 43.2% compared with that of the neat PLA/GSE-20 blend. In addition, the introduction of GSE brought shape memory and fluorescence properties to PLA. The shape memory property was mainly attributed to the following two factors, the improved toughness that afforded a large deformation for the PLA blend and the crosslinked GSE as a dispersed phase temporally stored the internal stress induced by deformation. PLA/GSE blends exhibited interesting fluorescence. As the increase in GSE loading, the fluorescence intensity increased. PLA/GSE-40 which contained 40% GSE by weight exhibited stronger fluorescence than the crosslinked GSE. The fluorescence was mainly from GSE, and the well compatibilized interface in polymer blend further enhanced the fluorescence. The PLA blend developed in this work possesses unique shape memory and fluorescence properties the conventional PLA does not have. This novel PLA blend may find certain advanced applications, such as 4D printing, soft actuators, implantable scaffold, fluorescent marker, monitoring the biodegradation process of PLA, and fluorescence probe,

CRediT authorship contribution statement

Shuai Zhang: Investigation, Validation, Writing - original draft. **Tuan Liu:** Conceptualization, Supervision, Methodology, Writing - original draft. **Baoming Zhao:** Validation, Investigation. **Christina**

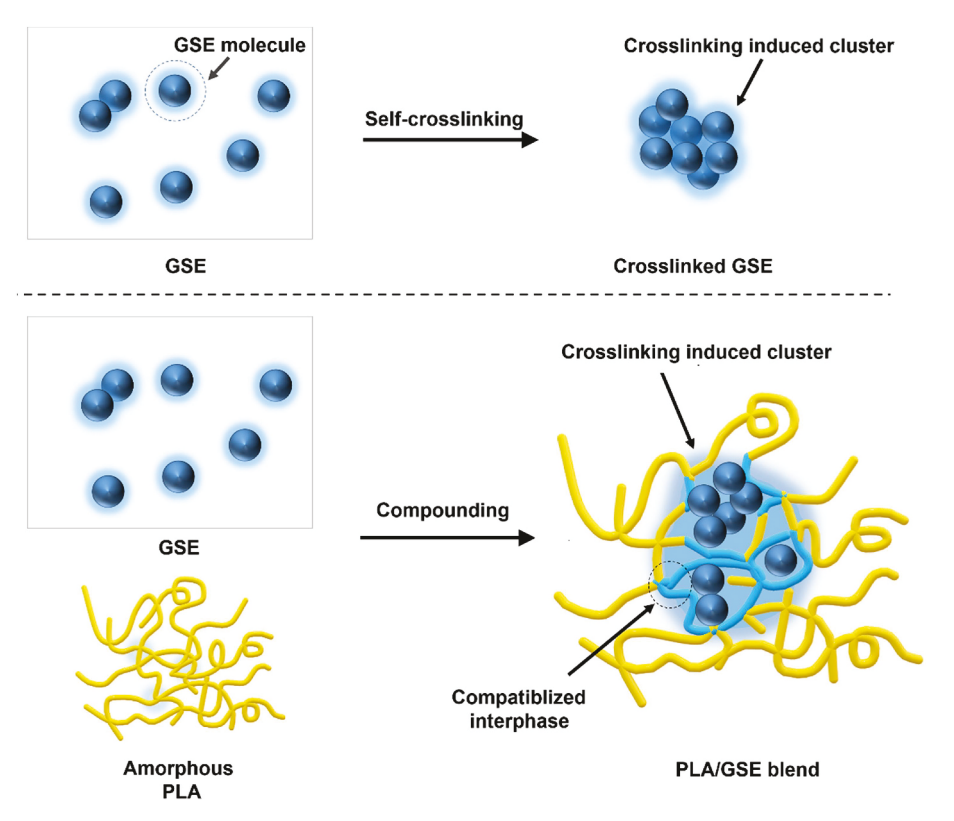


Fig. 6. The possible mechanism of crosslinking induced fluorescence in the PLA/GSE blends.

Verdi: Validation, Investigation. **Wangcheng Liu:** Validation, Investigation. **Cheng Hao:** Validation, Investigation. **Jinwen Zhang:** Conceptualization, Supervision, Writing - review & editing, Funding acquisition.

Declaration of competing interest

The authors declare that they have no known competing financial interests or personal relationships that could have appeared to influence the work reported in this paper.

Acknowledgements

The authors are grateful for the financial support from the Center for Bioplastics and Biocomposites (CB²).

Appendix A. Supplementary data

Supplementary data to this article can be found online at https://doi.org/10.1016/j.polymer.2020.122980.

References

- T. Xie, I.A. Rousseau, Facile tailoring of thermal transition temperatures of epoxy shape memory polymers, Polymer 50 (8) (2009) 1852–1856, https://doi.org/ 10.1016/j.polymer.2009.02.035.
- [2] T. Tsujimoto, H. Uyama, Full biobased polymeric material from plant oil and poly (lactic acid) with a shape memory property, ACS Sustain. Chem. Eng. 2 (8) (2014) 2057–2062. https://doi.org/10.1021/sc500310s.
- [3] Y. Chen, D. Yuan, C. Xu, Dynamically vulcanized biobased polylactide/natural rubber blend material with continuous cross-linked rubber phase, ACS Appl. Mater. Interfaces 6 (6) (2014) 3811–3816. https://doi.org/10.1021/am5004766.
- [4] Y. Feng, G. Zhao, J. Yin, W. Jiang, Reactive compatibilization of high-impact poly (lactic acid)/ethylene copolymer blends catalyzed by N, N-dimethylstearylamine, Polym. Int. 63 (7) (2014) 1263–1269, https://doi.org/10.1002/pi.4632.
- [5] L. Wang, W. Ma, R. Gross, S. McCarthy, Reactive compatibilization of biodegradable blends of poly (lactic acid) and poly (ε-caprolactone), Polym. Degrad. Stabil. 59 (1-3) (1998) 161–168, https://doi.org/10.1016/S0141-3910
- [6] D. Bryant, D. Greenfield, The use of fluorescent probes for the detection of underfilm corrosion, Prog. Org. Coating 57 (4) (2006) 416–420, https://doi.org/ 10.1016/j.porgcoat.2006.09.027.
- [7] S. Roshan, A.A.S. Dariani, J. Mokhtari, Monitoring underlying epoxy-coated St-37 corrosion via 8-hydroxyquinoline as a fluorescent indicator, Appl. Surf. Sci. 440 (2018) 880–888, https://doi.org/10.1016/j.apsusc.2018.01.188.
- [8] J. Tavakoli, H.-p. Zhang, B.Z. Tang, Y. Tang, Aggregation-induced emission lights up the swelling process: a new technique for swelling characterisation of hydrogels, Mater. Chem. Front. 3 (4) (2019) 664–667, https://doi.org/10.1039/c9qm00054b.
- [9] H. Zhang, Z. Zhao, P.R. McGonigal, R. Ye, S. Liu, J.W.Y. Lam, R.T.K. Kowk, W. Z. Yuan, J. Xie, A.L. Rogach, B.Z. Tang, Clusterization-triggered emission: uncommon luminescence from common materials, Mater. Today 32 (2020) 275–292, https://doi.org/10.1016/j.mattod.2019.08.010.
- [10] D. Wu, Y. Liu, C. He, S.H. Goh, Blue photoluminescence from hyperbranched poly (amino ester)s, Macromolecules 38 (24) (2005) 9906–9909, https://doi.org/ 10.1021/ma051407x.
- [11] W.I. Lee, Y. Bae, A.J. Bard, Strong blue photoluminescence and ECL from OHterminated PAMAM dendrimers in the absence of gold nanoparticles, J. Am. Chem. Soc. 126 (27) (2004) 8358–8359, https://doi.org/10.1021/ja0475914.
- [12] S. Niu, H. Yan, S. Li, C. Tang, Z. Chen, X. Zhi, P. Xu, A multifunctional silicon-containing hyperbranched epoxy: controlled synthesis, toughening bismaleimide and fluorescent properties, J. Mater. Chem. C 4 (28) (2016) 6881–6893, https://doi.org/10.1039/C6TC02546C.
- [13] S. Niu, H. Yan, Z. Chen, S. Li, P. Xu, X. Zhi, Unanticipated bright blue fluorescence produced from novel hyperbranched polysiloxanes carrying unconjugated carbon–carbon double bonds and hydroxyl groups, Polym. Chem. 7 (22) (2016) 3747–3755, https://doi.org/10.1039/C6PY00654J.
- [14] T. Liu, Y. Meng, X. Wang, H. Wang, X. Li, Unusual strong fluorescence of a hyperbranched phosphate: discovery and explanations, RSC Adv. 3 (22) (2013) 8269–8275, https://doi.org/10.1039/C3RA22680H.
- [15] X. Miao, T. Liu, C. Zhang, X. Geng, Y. Meng, X. Li, Fluorescent aliphatic hyperbranched polyether: chromophore-free and without any N and P atoms, Phys. Chem. Chem. Phys. 18 (6) (2016) 4295–4299, https://doi.org/10.1039/ C5CP07134H
- [16] Y. Du, H. Yan, W. Huang, F. Chai, S. Niu, Unanticipated strong blue photoluminescence from fully biobased aliphatic hyperbranched polyesters, ACS Sustain. Chem. Eng. 5 (7) (2017) 6139–6147, https://doi.org/10.1021/ acssuschemeng.7b01019.

- [17] X. Chen, Z. He, F. Kausar, G. Chen, Y. Zhang, W.Z. Yuan, Aggregation-induced dual emission and unusual luminescence beyond excimer emission of poly (ethylene terephthalate), Macromolecules 51 (21) (2018) 9035–9042, https://doi.org/ 10.1021/acs.macromol.8b01743.
- [18] Y. Tanaka, H. Kakiuchi, Study of epoxy compounds. Part VI. Curing reactions of epoxy resin and acid anhydride with amine, acid, alcohol, and phenol as catalysts, J. Polym. Sci. A. 2 (8) (1964) 3405–3430, https://doi.org/10.1002/ pol.1964.100020804.
- [19] Y. Tanaka, H. Kakiuchi, Study of epoxy compounds. Part I. curing reactions of epoxy resin and acid anhydride with amine and alcohol as catalyst, J. Appl. Polym. Sci. 7 (3) (1963) 1063–1081, https://doi.org/10.1002/app.1963.070070322.
- [20] T. Liu, S. Zhang, C. Hao, C. Verdi, W. Liu, H. Liu, J. Zhang, Glycerol induced catalyst-free curing of epoxy and vitrimer preparation, Macromol. Rapid Commun. 40 (7) (2019) 1800889, https://doi.org/10.1002/marc.201800889.
- [21] H. Fang, F. Jiang, Q. Wu, Y. Ding, Z. Wang, Supertough polylactide materials prepared through in situ reactive blending with PEG-based diacrylate monomer, ACS Appl. Mater. Interfaces 6 (16) (2014) 13552–13563, https://doi.org/10.1021/ am5027350
- [22] W. Li, Y. Zhang, J. Yang, J. Zhang, Y. Niu, Z. Wang, Thermal annealing induced enhancements of electrical conductivities and mechanism for multiwalled carbon nanotubes filled poly(ethylene-co-hexene) composites, ACS Appl. Mater. Interfaces 4 (12) (2012) 6468–6478, https://doi.org/10.1021/am302597f.
- [23] L. Deng, C. Xi, S. Ding, H. Fang, X. Wang, Z. Wang, Processing a supertoughened polylactide ternary blend with high heat deflection temperature by melt blending with a high screw rotation speed, Ind. Eng. Chem. Res. 58 (2019) 10618–10628, https://doi.org/10.1021/acs.iecr.9b01970.
- [24] L. Jiang, J. Zhang, M.P. Wolcott, Comparison of polylactide/nano-sized calcium carbonate and polylactide/montmorillonite composites: reinforcing effects and toughening mechanisms, Polymer 48 (26) (2007) 7632–7644, https://doi.org/ 10.1016/j.polymer.2007.11.001.
- [25] M.R. Aghjeh, M. Nazari, H.A. Khonakdar, S.H. Jafari, U. Wagenknecht, G. Heinrich, In depth analysis of micro-mechanism of mechanical property alternations in PLA/ EVA/clay nanocomposites: a combined theoretical and experimental approach, Mater. Des. 88 (2015) 1277–1289, https://doi.org/10.1016/j. matdes.2015.09.081.
- [26] Q. Wang, J. Zhang, X. Wang, Z. Wang, Significant enhancement of notched Izod impact strength of PLA-based blends through encapsulating PA11 particles of low amounts by EGMA elastomer, Appl. Surf. Sci. 526 (2020) 146657.
- [27] V. Ojijo, S. Sinha Ray, R. Sadiku, Toughening of biodegradable polylactide/poly (butylene succinate-co-adipate) blends via in situ reactive compatibilization, ACS Appl. Mater. Interfaces 5 (10) (2013) 4266–4276, https://doi.org/10.1021/ am400482f.
- [28] K. Zhang, V. Nagarajan, M. Misra, A.K. Mohanty, Supertoughened renewable PLA reactive multiphase blends system: phase morphology and performance, ACS Appl. Mater. Interfaces 6 (15) (2014) 12436–12448, https://doi.org/10.1021/ am50233711.
- [29] X. Meng, V. Bocharova, H. Tekinalp, S. Cheng, A. Kisliuk, A.P. Sokolov, V. Kunc, W. H. Peter, S. Ozcan, Toughening of nanocelluose/PLA composites via bio-epoxy interaction: mechanistic study, Mater. Des. 139 (2018) 188–197, https://doi.org/10.1016/j.matdes.2017.11.012.
- [30] X. Hao, J. Kaschta, Y. Pan, X. Liu, D.W. Schubert, Intermolecular cooperativity and entanglement network in a miscible PLA/PMMA blend in the presence of nanosilica, Polymer 82 (2016) 57–65, https://doi.org/10.1016/j. polymer.2015.11.029.
- [31] E.J. Dil, B.D. Favis, Localization of micro- and nano-silica particles in heterophase poly(lactic acid)/poly(butylene adipate-co-terephthalate) blends, Polymer 76 (2015) 295–306, https://doi.org/10.1016/j.polymer.2015.08.046.
- [32] F. Jiang, C. Fang, J. Zhang, W. Wang, Z. Wang, Triblock copolymer elastomers with enhanced mechanical properties synthesized by RAFT polymerization and subsequent quaternization through incorporation of a comonomer with imidazole groups of about 2.0 mass percentage, Macromolecules 50 (16) (2017) 6218–6226, https://doi.org/10.1021/acs.macromol.7b01414.
- [33] J. Huang, L. Cao, D. Yuan, Y. Chen, Design of multi-stimuli-responsive shape memory biobased PLA/ENR/Fe₃O₄ TPVs with balanced stiffness-toughness based on selective distribution of Fe₃O₄, ACS Sustain. Chem. Eng. 7 (2) (2018) 2304–2315, https://doi.org/10.1021/acssuschemeng.8b05025.
- [34] W. Wang, P. Ping, X. Chen, X. Jing, Polylactide-based polyurethane and its shape-memory behavior, Eur. Polym. J. 42 (6) (2006) 1240–1249, https://doi.org/10.1016/j.eurpolymj.2005.11.029.
- [35] J. Li, X. Zhao, L. Ye, P. Coates, F. Caton-Rose, Multiple shape memory behavior of highly oriented long-chain-branched poly (lactic acid) and its recovery mechanism, J. Biomed. Mater. Res. A. 107 (4) (2019) 872–883, https://doi.org/10.1002/jbm.
- [36] W. Zhang, L. Chen, Y. Zhang, Surprising shape-memory effect of polylactide resulted from toughening by polyamide elastomer, Polymer 50 (5) (2009) 1311–1315, https://doi.org/10.1016/j.polymer.2009.01.032.
- [37] F.S. Senatov, K.V. Niaza, M.Y. Zadorozhnyy, A.V. Maksimkin, S.D. Kaloshkin, Y. Z. Estrin, Mechanical properties and shape memory effect of 3D-printed PLA-based porous scaffolds, J. Mech. Behav. Biomed. 57 (2016) 139–148, https://doi.org/10.1016/j.jmbbm.2015.11.036.
- [38] S. Zhu, Y. Song, J. Shao, X. Zhao, B. Yang, Non-conjugated polymer dots with crosslink-enhanced emission in the absence of fluorophore units, Angew. Chem. Int. Ed. 54 (49) (2015) 14626–14637, https://doi.org/10.1002/anie.201504951.
- [39] B. Liu, H. Zhang, S. Liu, J. Sun, X. Zhang, B.Z. Tang, Polymerization-induced emission, Mater. Horiz. (2020), https://doi.org/10.1039/c9mh01909j.